Optical determination of the band gap and band tail of epitaxial $Ag_2ZnSnSe_4$ at low temperature

Joël Bleuse,[1,*] Sylvain Perret,[1] Yoann Curé,[1] Louis Grenet,[2] Régis André,[3] and Henri Mariette[3]

[1]*Université Grenoble-Alpes, CEA-CNRS joint group "Nano-Physique & Semi-Conducteurs", CEA, IRIG, PHELIQS, 17 rue des martyrs, 38054 Grenoble CEDEX 9, France*

[2]*Université Grenoble-Alpes, CEA, LITEN, 17 rue des Martyrs, 38054 Grenoble CEDEX, France*

[3]*Université Grenoble-Alpes, CEA-CNRS joint group "Nano-Physique & Semi-Conducteurs", CNRS, Institut Néel, 25 rue des martyrs, 38042 Grenoble CEDEX 9, France*

(Received 7 July 2020; revised 15 October 2020; accepted 26 October 2020; published 19 November 2020)

We report on the precise determination, in $Ag_2ZnSnSe_4$ epitaxial layer, of both the band gap E_g and the characteristic Urbach energy U that describes the density of localized, defect states in the gap. Various origins for these defect band tail states have been considered, together with the corresponding modeling for their density of states, in order to fit the whole of the optical spectral data. The interest of the methodology developed here is to account quantitatively not only for the absorption and steady-state photoluminescence data but also for the time-resolved photoluminescence spectra. We compare the different origins of localized band tail states to select the standard textbook, Urbach tail model that corresponds to short-range band gap fluctuations. Such an approach is different from the one most often used to evaluate the energy extent of the localized states, which is the Stokes shift between the energies of the photoluminescence emission and the absorption threshold. The advantage of the present method is that no arbitrary choice of the low power excitation has to be done to select the photoluminescence emission spectrum and its peak energy. Thanks to this systematic study of both photoluminescence excitation and time-resolved photoluminescence spectra at low temperature (6 K), the values $E_g = 1226 \pm 5$ meV and $U = 20 \pm 3$ meV are found for this promising absorber for thin films photovoltaics.

DOI: 10.1103/PhysRevB.102.195205

I. INTRODUCTION

The occurrence of a band tail just below the band gap in the absorption spectra, when adding impurities to a pure crystal was first reported a long time ago by F. Urbach *et al.* [1] in AgCl crystals containing copper as an impurity. The observed band tail was well described by a single exponential and attributed to localized states created by the Cu-Ag cation disorder. Such analytic contribution to account for optical properties of doped semiconductors was then found to be verified and useful in a huge number of cases, especially when dealing with localized, substitutional impurities. More recently, as an example, the optical signature of impurity-impurity interactions in copper-containing II-VI alloy semiconductors has been identified by systematically comparing optical absorption and emission spectra [2]. We show here such an experimental, optical approach; we quantitatively analyze photoluminescence excitation data (reflecting the density of states) and time-resolved emission spectra (reflecting the evolution of the electron-hole population), using a single exponential shape for the localized states, as proposed by Urbach. This allows us to accurately determine the band gap and the energy extent of the band tail in the case of $Ag_2ZnSnSe_4$, a new promising material for solar energy conversion.

Indeed, by contrast to solar cells based on chalcopyrites such as $Cu(In, Ga)(S, Se)_2$ and zincblende structures (CdTe), for which a power conversion efficiency (PCE) above 20% has been achieved [3], kësterite-based solar cells such as $Cu_2ZnSn(S, Se)_4$ (CZTSSe) only reached 12.6% PCE [4]. This limited performance is mainly related to a large open-circuit voltage (V_{OC}) deficit, as evidenced by the above CZTSSe record cell, which attains only 59% of the Shockley-Queisser limit for V_{OC}, whereas it reaches 80% of this limit for both the short circuit current and the fill factor [4].

Several hypotheses have been drawn to explain such a V_{OC} limitation. Among them, the presence of a large band tail of localized states below the extended state bands is considered to be one of the main culprits, as it diminishes the effective band gap, and consequently the available V_{OC} [5]; it also induces the localization of charge carriers, and thereby reduces their collection efficiency in devices.

The importance of such band tails in these kinds of materials (chalcopyrites, kësterites, stannites) has been discussed extensively in the literature [5–12]. Band tailing in semiconductors arises from either spatial band gap variations—coming from crystalline, compositional inhomogeneities, including some local disorder that induces the formation of *neutral* defects and clusters, or electrostatic potential fluctuations—due to high concentration of *charged* defects. In the latter case, by contrast to the former, there is no spatial variation of E_g, but the regions containing electrons or holes are spatially separated, and sub-band gap

*joel.bleuse@cea.fr

absorption is only possible because of efficient tunneling effects [5,12].

Both effects lead to nonzero density of states (DoS) within the band gap. Depending on the works, authors reported in CIGSe and CZTSe on the predominance of either band gap fluctuations [6,8,11] or electrostatic fluctuating potentials [5,9,12]. Most however note that by fitting the sub-band tail experimental data, it is often difficult to discriminate between the different origins of these localized states. In any case, the potential cause for band gap fluctuations and electrostatic potential fluctuations in kësterites is related to the occurrence of high concentration of antisite defects—in other words, of Cu-Zn disorder.

The presence of large densities of intrinsic native point defects, as predicted by density functional theory (DFT) calculations [13–15], can directly influence the generation, separation and recombination of photogenerated electron-hole pairs. For CZTSSe, a large density of acceptor Cu_{Zn} antisites and Cu vacancies V_{Cu} has been calculated, given that both these point defects have the lowest formation energies [13]. Moreover, these point defects are stabilized by the formation of self-compensated neutral defect complexes made of triplets of exchange atoms such as $[2Cu_{Zn} + Sn_{Zn}]$. In other words, the disorder in the cation sublattice, especially between Cu and Zn, strongly influences the occurrence of such defect clusters [14,15], and is then directly responsible for the presence of potential fluctuations [16]: large amounts of these defects are likely to form band tailing, and believed to be one of the main reasons for the V_{OC} deficit [5,8]. This issue is of particular importance, which is why we pursued our optical investigation in depth.

Such band tails have been studied qualitatively by optical spectroscopy: mainly photoluminescence (PL) as a function of temperature and excitation power [17–23], but also by PL excitation spectroscopy (PLE), which reveals the density of states in the presence of potential fluctuations [24,25], and by time-resolved photoluminescence spectroscopy (TR-PL), which gives information about the localization and transfer of carriers between the band tail states, as was done on CZTS single crystals [22,25]: all these data have been analyzed as a function of the order/disorder degree in the quaternary structure [25,26].

The substitution of copper by silver is one of the proposed methods to reduce the density of defect states. The motivation for $Ag_2ZnSnSe_4$ (AZTSe) or $(Cu_{2-x}Ag_x)ZnSnSe_4$ derives from the reduced Ag_{Zn} antisite concentration that was theoretically predicted by DFT calculations, as a consequence of a much larger formation energy [27–29] for Ag_{Zn} than for Cu_{Zn} antisites. Then, if the antisite defects between atoms of columns I and II of the periodic table are indeed the main cause of band tailing, $Ag_2ZnSnSe_4$ has the potential to significantly reduce the problem and to allow for larger V_{OC}.

Such a substitution was successfully used [30–32] to observe an improved efficiency, mainly due to a 8%–10% improvement of V_{OC} as compared to the baseline CZTSSe device. More precisely, it has been estimated, from room temperature optical data, that the band tailing effect is dramatically suppressed for AZTSe (pure-Ag) samples [31].

In this work, we study single crystal, stoichiometric $Ag_2ZnSnSe_4$ epilayers, as they offer a way to reduce the ambiguity on the nature of defects by eliminating grain boundaries. Complementary, low temperature optical experiments are compared: (i) the variation of the PLE intensity as a function of excitation photon energy; (ii) the evolution in time and energy of the TR-PL emission after a short pulse excitation; and (iii) the variations of PL spectra with excitation power density. All these data are analyzed with a quantitative model that enables us to accurately determine both the band gap and the energy extent of the localized states band tail, which appears just below the band gap: the latter can be characterized by a Urbach energy U, and is probably dominated in our samples by local band gap fluctuations rather than electrostatic ones. These experimental data also evidence the transfer mechanisms that occur between the localized states, within this band tail.

II. EXPERIMENTAL MEASUREMENTS

The samples are grown in a MBE chamber using four Knudsen cells for Ag, Zn, Sn, and Se, without post treatment of the layer. The beam equivalent pressures of the four elements were measured by a gauge pressure meter positioned at the location of the sample. The AZTSe layers are grown on a (001) InAs substrate kept at a temperature of 460 °C with a growth rate of 4 nm per minute. X-ray diffraction and Raman spectroscopy are used to check the absence of secondary phases, as was done on CZTSe [33].

For optical spectroscopy, both steady-state and time-resolved microphotoluminescence experiments are carried out at cryogenic temperatures (6 K) in a helium-flow, optical cryostat. Electron-hole pair injection in the AZTSe layer is provided by a Ti:sapphire laser (Coherent Mira), operating either in steady-state mode or in pulsed mode with 200 fs-long pulses, and a repetition rate set by a cavity dumper at either 246 kHz (extracting one pulse every 222) or 501 kHz (every 109). The laser excitation is focused down to a 1.5-μm diameter spot on the sample with the same microscope objective (0.4 numerical aperture) that collects the luminescence signal. For PLE experiments, the excitation source is a 1 kW, halogen lamp coupled to a monochromator. The emission of the AZTSe layer is then spectrally dispersed by a 640-mm focal length monochromator and detected by a silicon CCD (Andor DU420A-BRDD, for steady-state PL and PLE) or a silicon avalanche photodiode (Perkin-Elmer SPCM AQR-15, for TR-PL).

Low-temperature TR-PL spectra are measured at a series of about 20 different photon energies, evenly spaced from 1100 to 1370 meV, over a time window of about 600 ns, with 50-ps time bins. This gives a full view over the relaxation and recombination processes involved in the $Ag_2ZnSnSe_4$ sample. For each of the nearly 12000 time bins, a low-resolution PL spectrum is therefore available for analysis. The temporal instrument response of the TR-PL setup, measured with the excitation laser pulses, presents a time resolution of about 400 ps, which is associated with the time jitter of the avalanche photodiode. To provide a clean measurement of the PL decay, the TR-PL measurements are conducted at a 3-μW average pumping power.

III. DENSITY OF STATES MODELING

The DoS of such semiconductor materials is the combination of the DoS of an ideal direct band gap semiconductor—a square root DoS in the band—with a sub-band gap DoS, related to localized states, that, in line with the literature [12], we chose to express with the general mathematical functional form:

$$d_\beta(E) = \begin{cases} A\sqrt{\frac{E-E_g}{U}} & \text{if } E \geqslant E_1 \\ B\,\exp\left[-\left(C - \frac{E-E_g}{U}\right)^\beta\right] & \text{if } E \leqslant E_1 \end{cases},$$

where β and U characterize the shape of the tail states DoS within the gap for the localized carriers and E_g is the band gap for the band to band, free-carrier transitions. Since the experimental data show no hints of any singularity at any energy, we assumed that both the DoS $d_\beta(E)$ and its derivative are continuous functions at the E_1 "connecting" energy. These assumptions lead to $E_1 = E_g + U/2$, whatever the β value, and to the following functional form for $d_\beta(E)$, if $E \geqslant E_g + U/2$:

$$d_\beta(E) = A\sqrt{2\frac{E-E_g}{U}}, \quad (1)$$

and, if $E \leqslant E_g + U/2$:

$$d_\beta(E) = A\exp\left[\beta^{\frac{\beta}{1-\beta}} - \left(\beta^{\frac{1}{1-\beta}} + \frac{1}{2} - \frac{E-E_g}{U}\right)^\beta\right], \quad (2)$$

which is valid if $\beta \neq 1$. In the limit $\beta \to 1$, this last equation (2) becomes

$$d_1(E) = A\exp\left(\frac{E-E_g}{U} - \frac{1}{2}\right).$$

Various values of β have been considered, depending on the mechanism at the origin of the tailing behavior, and give rise to various characteristic energies U for the band tail: (i) $\beta = 1$ corresponds to the more general case and is described as Urbach tails [1]; its classical interpretation considers localized band tail states, within the forbidden gap, as due to local disorder such as statistical A-B local configurations in $A_xB_{1-x}C$ alloys, i.e., Ag-Zn disorder for our AZTSe compound; (ii) $\beta = 5/4$ has been deduced in the scope of electrostatic fluctuations induced by charge defects with a spatial range smaller than the screening length, and with a random distribution of these defects [5,12,34]; (iii) $\beta = 3/2$ is also obtained when considering heavily doped semiconductors, [35] in which a Franz-Keldysh effect—i.e., the tunneling in the presence of local internal electric field created by the charge impurities—is dominant; and (iv) $\beta = 2$ has been found for band gap fluctuations with a model assuming a Gaussian distribution of local band gaps with a given standard deviation [5,6,8,11].

In principle, fitting the experimental data with these different analytic functions should allow us to distinguish unequivocally between any particular type of fluctuating potentials [9]. However, there are two kinds of strong limits for such an approach: (i) conceptually, as pointed out by Katahara *et al.* [12], there is no bijection between the analytic model and the underlying tailing mechanism, e.g., a β value of 2 is found for band gap fluctuations [6,11], but also in the case of the Thomas-Fermi approach that consider electrostatic fluctuations with a characteristic energy proportional to the square root of the charge impurity concentration [12]; and (ii) by comparing only the experimental data of the DoS (absorption or PLE) with the above functions, there is not always a clear discrimination between the various mathematical functions. This last point is illustrated in the present work, in Sec. IV. For this reason, we report here on the modeling of not only the PLE data, but also of the PL emission spectra (steady-state and time-resolved). To account quantitatively for the latter, we consider the product of the DoS given by equations (1,2) with a Fermi occupation function, in order to keep track of the state filling processes, without any other assumption.

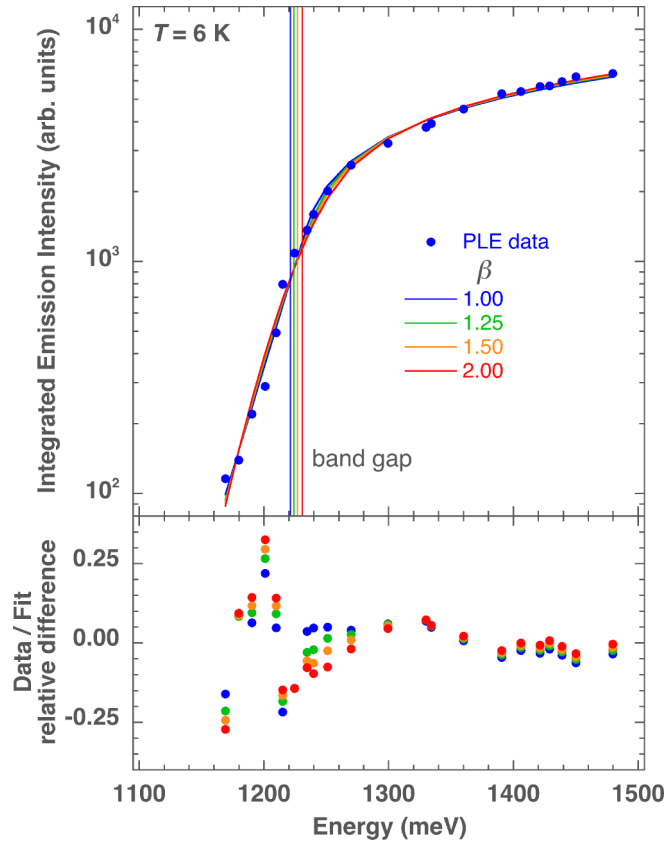

FIG. 1. Top: PLE experimental data (blue dots) at 6 K. The integrated emission intensity is detected in the 1.05–1.09 eV energy range as a function of the excitation photon energy. Least squares fits of the model DoS $d_\beta(E)$ (solid, colored lines) yield values for the band gap E_g and band tail characteristic energy U shown in table I. Each colored vertical line points to the band gap value obtained for the fit of the same color/β value. (Bottom) Relative difference—for each data point—between data and fit values, with the same color correspondence to the model parameter β as in the top frame.

IV. PHOTOLUMINESCENCE EXCITATION

PLE experiments allow us to measure the threshold of the optical absorption, for the direct evaluation of the AZTSe band gap at low temperature. Figure 1 shows the PLE integrated emission intensity for the detection energy window spanning from 1.05 to 1.09 eV. Knowing that, in a PLE measurement, we detect the emitted signal at a fixed, given

TABLE I. Band gap E_g, and tail extension characteristic energy U, as a function of the fit parameter β. The fit error is the sum—over all data points—of the square of the relative error (shown in the bottom frame of Fig. 1).

β	E_g /meV	U /meV	Fit error
1.00	1221.2	24.5	0.185
1.25	1224.1	34.1	0.216
1.50	1226.8	44.9	0.253
2.00	1230.8	69.6	0.307

energy window while scanning the energy of the excitation light, it is well known that such a spectrum does not simply reflect the absorption spectrum, but also includes the variations of the efficiency of the relaxation from the absorption final state to the emission initial state. To ascertain that the PLE spectra are essentially proportional to the absorption coefficient [36], the efficiency of the relaxation process should be nearly constant, whatever the detection energy (i.e., whatever the states involved in the emission process). We checked, experimentally, that this assumption is verified, by measuring the PLE spectra at various detection energies, within the broad emission line [25]: up to a global scale factor, these spectra are indeed identical, within a few meV.

The band gap is therefore estimated from fitting the PLE data with the model DoS functions $d_\beta(E)$, which are presented in the DoS modeling section. The least squares fit of the experimental data are shown in Fig. 1 for the usually considered values of β [12]. The corresponding values for E_g and U are reported in table I, together with the value of the—minimized—fit error.

Two conclusions are clearly deduced from this systematic analysis. (i) It is hardly possible to discriminate a model β value by only fitting the PLE experimental data, since the variations in fit error come from only a few low-signal data points (see Fig. 1 and Table I); to first order, this shows that the origin of the fluctuating potentials is difficult to determine. (ii) The average band gap—over the four β values—is $E_g = 1226$ meV, with a 5-meV maximum deviation. Our determination of E_g is therefore not model-dependent.

By contrast to E_g, the values obtained for U clearly depend on the β parameter value. One must however note that the physical meaning of U is model-dependent, i.e., depends on the value of β.

If we compare the general functional form given by equations (1) and (2) with the expressions of existing models for sub-band gap absorption [12], we see that: U is the "standard," so-called Urbach energy for $\beta = 1$; $U = (25\pi/4 \cdot N_t a^3)^{2/5} E_0$ for $\beta = 5/4$, where E_0 is the impurity binding energy; for $\beta = 3/2$, $U = (9/2\,(\hbar e\mathcal{E})^2/m_e^*)^{1/3}$, where $\mathcal{E}$ is the internal electric field due to the charged impurity distribution; and for $\beta = 2$, $U = \sqrt{2}\sigma$, where σ is the root-mean-square depth of the potential well created by the local band gap fluctuations.

V. TIME-RESOLVED PHOTOLUMINESCENCE

Another way to estimate the band gap, and the extent of the band tail of localized states just below, is to perform a study of TR-PL spectra [5,25]. These spectra are reported in Fig. 2 for various time delays after a 1.55 eV ≈200-fs long, pulsed excitation [37]. In Fig. 2(a), the rise of the TR-PL signal is plotted on a linear scale, which shows a maximum intensity at a 0.90-ns delay: this should correspond to the fast relaxation of the energy of hot carriers within the bands. Then, in Fig. 2(b), the subsequent signal decay exhibits a red energy shift that increases with time. This reveals the transfer of carriers within a band tail of states below the band gap, from the highest states to the lowest ones, on a much longer time scale—of the order of 100 ns.

These transfers between states of differing energies explain why, in such a case, a decay curve measured at a single photon energy can only accidentally give rise to a single exponential and would account for only meaningless characteristic transition times.

In the present case, the time-dependent spectra are plotted, on a semilogarithmic scale, for time delays in a geometric series.[1] In such a scheme, if the PL decay were following a power law dependence on time [38,39], the intensity maxima between two successive curves should be visually equidistant on this semilogarithmic plot: it is not the case here, at least for times up to ≈25 ns, as the larger the time, the closer the spectra look, which evidences that the PL intensity peak decrease is slower than any power law, therefore slower than any exponential. For times larger than ≈25 ns, the data are not so clear, and a power law behavior cannot be fully excluded.

From this, we can then infer that the carriers at the origin of the emission in the band tail are not fully independent, since the power law decay inherent to bimolecular recombination [38] is absent for delays below 25 ns. It is also worth mentioning here that, at room temperature, such a carrier redistribution in CZTSSe was found to occur over only a much shorter, 1 ns time scale, and on an energy range of only 10 meV [39].

To get a more quantitative account of our data, we use the following analysis methodology: each of these low-resolution, TR-PL spectra is fitted with a function that is the product of the above density of states $d_\beta(E)$ (1,2) with a Fermi occupation function:

$$f(E) = \left[1 + \exp\left(\frac{E - E_F}{k_B T}\right)\right]^{-1} \quad (3)$$

For each value of β, we first test the fit of the TR-PL spectra over a sequence of delay ranges (1.6–5, 5–10, and 10–15 ns). The fitting procedure is two-step: for each range, we compute a global error over all of the TR-PL spectra in the range, assuming a constant value for the tail extension parameter U; then, this global error is minimized by letting U vary. These fits for $\beta > 1$ give rise to nonmonotonic variations of U with delay range (see Ref. [37] for the TR-PL fits with $\beta = 1.25, 1.5, 2$): only $\beta = 1$ gives out a nearly constant U value (19.6 ± 2 meV) over the three delay ranges.

In addition, looking carefully at the low energy side of the TR-PL spectra, one sees that they all exhibit a simple

[1]Figure 2(b) shows nine spectra for delays from 1 to 200 ns, geometrically "equidistant," i.e., for delays separated by a factor $200^{1/8} \approx 1.939$, rounded to the time resolution, which is here the time bin width: 50 ps.

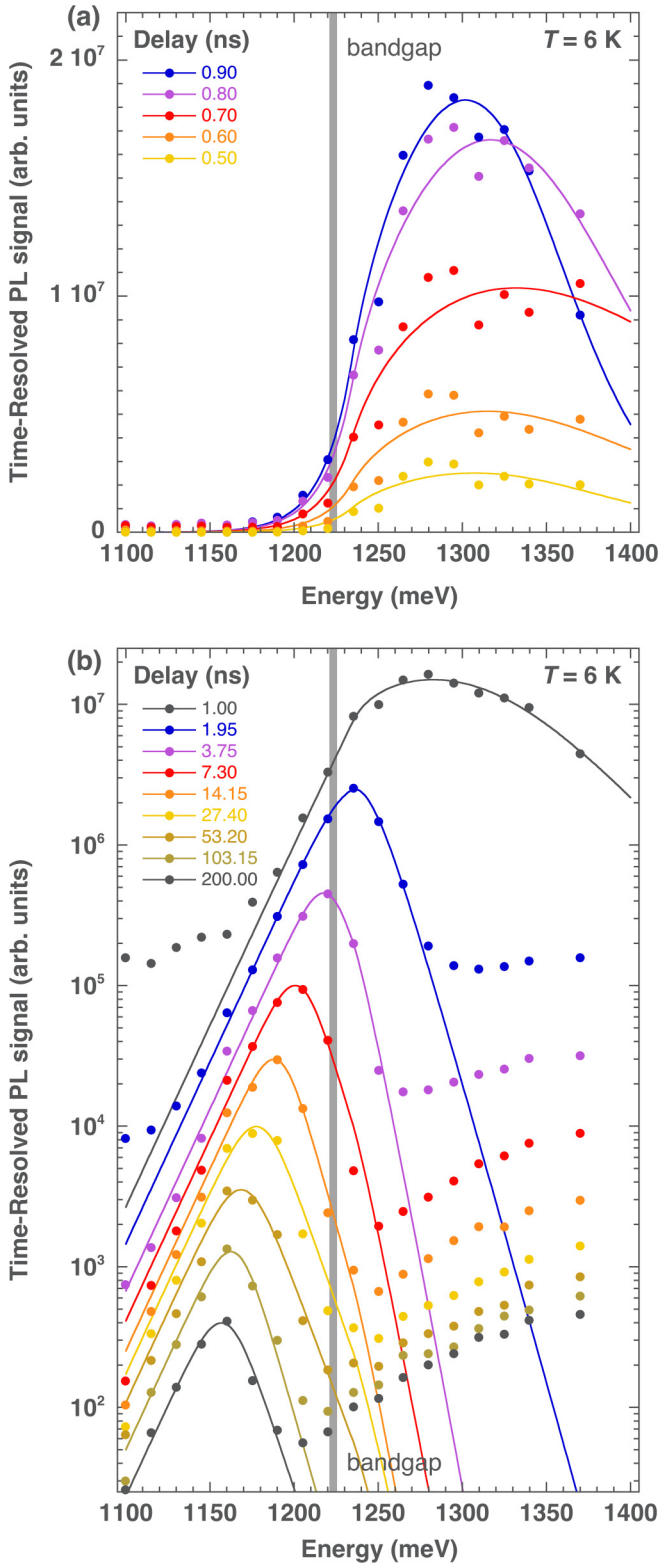

FIG. 2. Low-temperature TR-PL spectra. Experimental data (dots) and fitting curves (solid lines) for various time delays after the pulse excitation. (a) Signal rise for short delays, on a linear scale. The TR-PL signal peak is maximum at a 0.90 ns delay. (b) Signal decay, on a semilogarithmic scale. TRPL spectra exhibit red energy shifts that increase with time, revealing the transfer of carriers within the band, up to ≈2 ns, and between the localized states in the band tail, for longer delays. In both frames, the gray vertical line covers the band gap E_g values between those fitted from the PLE (1221 meV) and TR-PL data (1226 meV).

exponential behavior—i.e., a straight line in semilogarithmic scale—over more than two orders of magnitude, with the same characteristic energy decay U, whatever the time delay between 2 and 200 ns after the excitation pulse [37]: these experimental features can only be properly described by the exponential model, i.e., $\beta = 1$. This, together with the inconsistency of the $\beta > 1$ fits, lead us to chose the Urbach-like, exponential model, to account for our data.

Knowing from the PLE data that E_g weakly depends on β, and from the TR-PL data that U is constant only for $\beta = 1$, whatever the time, we complete a second, two-step fitting procedure with $\beta = 1$, as follows: the nearly 2000 spectra, from 0.50 to 100 ns after the excitation pulse, are fitted[2] with the function $f(E)d_1(E)$, keeping the values of E_g and U constant, with only 3 parameters varying with time: A, E_F, and k_BT. The cumulated errors between data and fitted values over these 2000 spectra then represent a global error for the chosen (E_g, U) pair. This is then repeated to find the optimal E_g and U values that minimize this global error.[3]

The results of this last procedure are given in Fig. 2, showing the fits (full lines) together with experimental data (points): a bandgap $E_g = 1226 \pm 3$ meV, and an Urbach tail characteristic energy $U = 17 \pm 3$ meV are found, along with the time variation of the parameters A, E_F, and k_BT. This determination of E_g and U is in good agreement with the one deduced above from the PLE experiments.

One must however take note that we do not currently understand the exact nature of the emission that is always observed on the high energy side of the spectra ($E > 1.3$ eV); this emission is also observed in steady-state PL spectra (see Fig. 3). As it is clearly distinguished from the emission peak, it is not taken into account in our data analysis.

VI. DISCUSSION

It is clear from this analysis that the maxima of the TR-PL peak, for very short time delays after the pulse, are at energies larger than E_g [Fig. 2(a)], and correspond to the recombination of hot carriers, before and along energy relaxation from phonon emission. On the other hand, for delays larger than ≈3 ns, the maxima of the TR-PL peak occur at energies lower than E_g, and are related to carrier recombination involving localized states in the band tail.

Considering the parameters extracted from the model, the Fermi energy E_F is—for delays larger than 1 ns—a decreasing function of time that closely follows the peak energy maxima, as expected from the characteristics of our model function $f(E)d_1(E)$. This superposition of E_F with the energy variation of the peak maxima is confirmed with steady-state PL spectra as a function of power excitation (see Fig. 3). There, by varying the power density over five orders of magnitude, the PL maxima are shifted by ≈100 meV, from 1145 to 1245 meV, as are the values of E_F (see Fig. 4).

[2]The function `scipy.optimize.curve_fit`, from package SCIPY 1.4.1, is used with a Levenberg-Marquardt algorithm [40].

[3]The minimization search goes over the rectangle [1200; 1250] × [4; 24] meV^2, where a single global minimum is found at (1226.3; 16.8) meV.

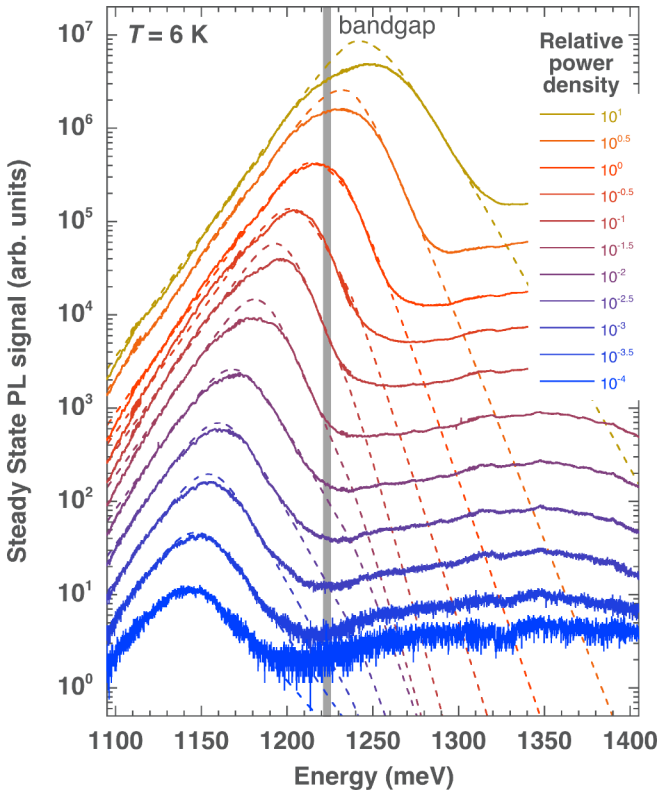

FIG. 3. Steady-state PL spectra as a function of excitation power—over five orders of magnitude, on a semilogarithmic scale. The dashed lines correspond to fits with the model function $f(E)d_1(E)$, taking the E_g and U values obtained from the TR-PL data; the E_F parameters extracted from these fits are reported in Fig. 4. The exponential decrease on the low energy side of the spectra correspond to the characteristic energy U of the Urbach tail density of localized defect states in the gap. The gray vertical line shows the band gap position, as in Fig. 2.

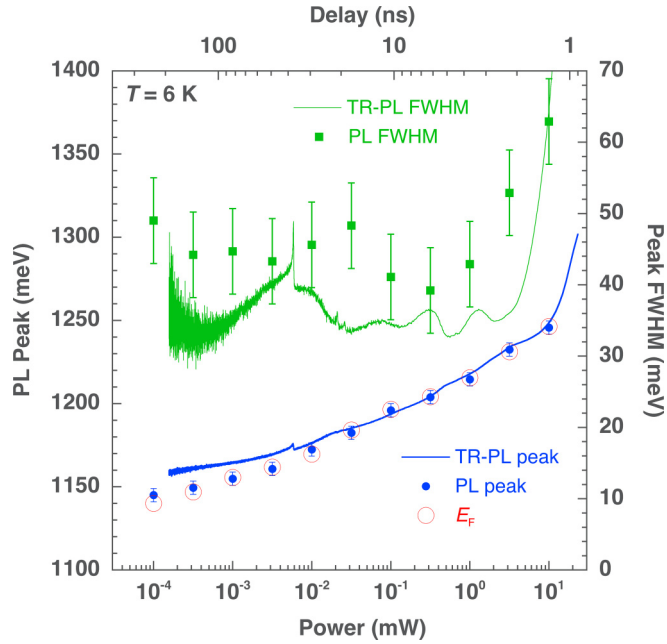

FIG. 4. Steady-state PL data as a function of excitation power (lower horizontal, logarithmic axis): the PL peak energy positions (blue dots, left vertical axis) are closely followed by the values of E_F (open red circles), which are deduced from the spectral fits in Fig. 3; the experimental values of the FWHM are also reported (green squares, right vertical axis). Superimposed are TR-PL data as a function of time delay (upper horizontal, logarithmic axis): the TR-PL peak energy positions (blue curve, left vertical axis), and peak FWHM (green curve, right vertical axis) are taken from the fitted curves. The two horizontal, logarithmic axes give the correspondance between delay and excitation power, as both correspond to variations of the electron-hole density. The "jump" in TR-PL curves around 36 ns delay comes from a weak, parasitic re-excitation.

In both sets of experimental data—steady-state PL as a function of power excitation and TR-PL, the emission spectra can be related to the steady-state or instantaneous carrier density. PL peak and Fermi energies, as well as carrier temperatures should therefore correspond when the carrier densities match. This correspondence is attempted in Fig. 4 where we adjust the excitation power and time scales to show that peak energy and full width at half maximum (FWHM) pairs exhibit similar trends between steady-state and time-resolved PL. This shows that, for delays larger than ≈5 ns, the carrier populations in TR-PL measurements are probably close to thermal equilibrium.

Our second fit parameter, the "temperature" k_BT, which is directly related to the peak FWHM, decreases as a function of time and saturates, at delays larger than 5 ns, to a value of ≈6 meV, which is equivalent to $T \approx 70$ K: this temperature, much larger than the bath one (6 K), shows the limitation of our model to account for weakly populated discrete defect states in the band tail. Nevertheless, these values of k_BT between 1 and 200 ns can be used to estimate the FWHM (full green line in Fig. 4), which shows values between 35 and 70 meV, fully accounting for the TR-PL experimental data. These are in very good agreement with the peak FWHM deduced from steady-state PL spectra (green squares), and a factor of 2 smaller than the FWHM usually measured on pure copper kësterites compounds [25,26], which lie between 70 and 110 meV, even for the most ordered CZTS monocrystalline samples.

VII. CONCLUSION

This work reports on a precise determination of the band gap of monocrystalline $Ag_2ZnSnSe_4$ at low temperature. Both photoluminescence excitation and time-resolved photoluminescence lead to a value of E_g at 6 K equal to 1226 ± 5 meV. It is worth noting that such values are much lower than the ones reported at room temperature for polycrystalline thin films: figuring diffuse reflectance data in a Tauc plot, W. Gong *et al.* [41] obtained a value of $E_g = 1.34$ eV, whereas Gershon *et al.* [42] deduced a value of 1.35 eV from External Quantum Efficiency data, in agreement with their room-temperature PL emission maximum. Variations of the gap values can however be strongly dependent on the selenization temperature, i.e., Se content, as pointed out by Jiang *et al.* [43] who reported band gap values between 1.33 and 1.59 eV, from absorption data. In any case, as pointed out by Siebentritt *et al.* [7], it is difficult to determine the band gap only from a

Tauc plot, when dealing with a large defect-related DoS in the gap. Further optical studies are under way to understand this apparent abnormal temperature dependence of the band gap.

This work also presents a quantitative methodology to precisely deduce the band gap E_g and the characteristic energy U for the extent of the tail of localized states, from the PLE and TR-PL data. Such an approach is different from the one usually used, namely measuring the energy shift between the PL emission and the absorption PLE threshold (the Stokes shift). The advantage of the present method is that no arbitrary choice of the low power excitation has to be done to select the PL emission spectrum and its peak energy, which could vary widely [see PL peak energies (blue dots) in Fig. 4].

Finally, with this systematic optical spectroscopy study and the above analysis methodology, the characteristic energy of the band tail in this new $Ag_2ZnSnSe_4$ material is found to be 20 ± 3 meV, which leads to a photoluminescence FWHM that is half those usually reported for even the most-ordered Cu-based kësterites compounds.

ACKNOWLEDGMENTS

This research was supported by the french ANR program "Carnot Energies du Futur," under the project name CAZTS. We also would like to thank the referees for bringing to our attention useful references on the modeling of defect band tails.

[1] F. Urbach, Phys. Rev. **92**, 1324 (1953); F. Moser and F. Urbach, **102**, 1519 (1956).
[2] B. Bhattacharyya, K. Gahlot, R. Viswanatha, and A. Pandey, J. Phys. Chem. Lett. **9**, 635 (2018).
[3] M. A. Green, Y. Hishikawa, E. D. Dunlop, D. H. Levi, J. Hohl-Ebinger, M. Yoshita, and A. W. Y. Ho-Baillie, Prog. Photovoltaics **27**, 3 (2019).
[4] W. Wang, M. T. Winkler, O. Gunawan, T. Gokmen, T. K. Todorov, Y. Zhu, and D. B. Mitzi, Adv. Energy Mater. **4**, 1301465 (2014).
[5] T. Gokmen, O. Gunawan, T. K. Todorov, and D. B. Mitzi, Appl. Phys. Lett. **103**, 103506 (2013).
[6] U. Rau and J. Werner, Appl. Phys. Lett. **84**, 3735 (2004).
[7] S. Siebentritt, G. Rey, A. Finger, D. Regesch, J. Sendler, T. P. Weiss, and T. Bertram, Sol. Energy Mater. Sol. Cells **158**, 126 (2016), Nanotechnology for Next Generation High Efficiency Photovoltaics Spring International School and Workshop, Spain, April 20–24, 2015.
[8] G. Rey, G. Larramona, S. Bourdais, C. Chone, B. Delatouche, A. Jacob, G. Dennler, and S. Siebentritt, Sol. Energy Mater. Sol. Cells **179**, 142 (2018).
[9] J. P. Teixeira, P. M. P. Salomé, B. Alves, M. Edoff, and J. P. Leitão, Phys. Rev. Appl. **11**, 054013 (2019).
[10] C. Malerba, M. Valentini, and A. Mittiga, Solar RRL **1**, 1700101 (2017).
[11] J. Mattheis, U. Rau, and J. H. Werner, J. Appl. Phys. **101**, 113519 (2007).
[12] J. K. Katahara and H. W. Hillhouse, J. Appl. Phys. **116**, 173504 (2014).
[13] S. Chen, A. Walsh, X.-G. Gong, and S.-H. Wei, Adv. Mater. **25**, 1522 (2013).
[14] S. Chen, J.-H. Yang, X.-G. Gong, A. Walsh, and S.-H. Wei, Phys. Rev. B **81**, 245204 (2010).
[15] S. Chen, L.-W. Wang, A. Walsh, X.-G. Gong, and S.-H. Wei, Appl. Phys. Lett. **101**, 223901 (2012).
[16] M. J. Romero, H. Du, G. Teeter, Y. Yan, and M. M. Al-Jassim, Phys. Rev. B **84**, 165324 (2011).
[17] K. Tanaka, Y. Miyamoto, H. Uchiki, K. Nakazawa, and H. Araki, Phys. Status Solidi A **203**, 2891 (2006).
[18] J. P. Leitão, N. M. Santos, P. A. Fernandes, P. M. P. Salomé, A. F. da Cunha, J. C. González, G. M. Ribeiro, and F. M. Matinaga, Phys. Rev. B **84**, 024120 (2011).
[19] X. Lin, A. Ennaoui, S. Levcenko, T. Dittrich, J. Kavalakkatt, S. Kretzschmar, T. Unold, and M. C. Lux-Steiner, Appl. Phys. Lett. **106**, 013903 (2015).
[20] S. Oueslati, G. Brammertz, M. Buffiere, C. Koeble, T. Oualid, M. Meuris, and J. Poortmans, Sol. Energy Mater. Sol. Cells **134**, 340 (2015).
[21] J. Sendler, M. Thevenin, F. Werner, A. Redinger, S. Li, C. Hagglund, C. Platzer-Bjorkman, and S. Siebentritt, J. Appl. Phys. **120**, 125701 (2016).
[22] M. Lang, C. Zimmermann, C. Krämmer, T. Renz, C. Huber, H. Kalt, and M. Hetterich, Phys. Rev. B **95**, 155202 (2017).
[23] M. Grossberg, J. Krustok, J. Raudoja, and T. Raadik, Appl. Phys. Lett. **101**, 102102 (2012); M. Grossberg, T. Raadik, J. Raudoja, and J. Krustok, Current Appl. Phys. **14**, 447 (2014).
[24] S. Siebentritt, N. Papathanasiou, and M. Lux-Steiner, Phys. Status Solidi B **242**, 2627 (2005).
[25] J. Bleuse, F. Ducroquet, and H. Mariette, J. Electron. Mater. **47**, 4282 (2018).
[26] K. Timmo, M. Kauk-Kuusik, M. Pilvet, T. Raadik, M. Altosaar, M. Danilson, M. Grossberg, J. Raudoja, and K. Emits, Thin Solid Films **633**, 122 (2017), 13th E-MRS Spring Meeting, Lille, France, May 02–06, 2016.
[27] T. Maeda, S. Nakamura, and T. Wada, *26th European Photovoltaic Solar Energy Conference (PV-SEC)* (2011), pp. 2836–2839, https://www.eupvsec-proceedings.com/proceedings?paper=12261.
[28] Z.-K. Yuan, S. Chen, H. Xiang, X.-G. Gong, A. Walsh, J.-S. Park, I. Repins, and S.-H. Wei, Adv. Funct. Mater. **25**, 6733 (2015).
[29] E. Chagarov, K. Sardashti, A. C. Kummel, Y. S. Lee, R. Haight, and T. S. Gershon, J. Chem. Phys. **144**, 104704 (2016).
[30] H. Cui, X. Liu, F. Liu, X. Hao, N. Song, and C. Yan, Appl. Phys. Lett. **104**, 041115 (2014).
[31] T. Gershon, Y. S. Lee, P. Antunez, R. Mankad, S. Singh, D. Bishop, O. Gunawan, M. Hopstaken, and R. Haight, Adv. Energy Mater. **6**, 1502468 (2016).
[32] C. J. Hages, M. J. Koeper, and R. Agrawal, Sol. Energy Mater. Sol. Cells **145**, 342 (2016).
[33] Y. Curé, S. Pouget, V. Reita, and H. Boukari, Scr. Mater. **130**, 200 (2017).

[34] S. Baranovskii, B. Shklovskii, and A. Efros, Sov. Phys. JETP-USSR **60**, 1031 (1984).
[35] P. Van Mieghem, Rev. Mod. Phys. **64**, 755 (1992).
[36] C. F. Klingshirn, Experimental methods, in *Semiconductor Optics* (Springer-Verlag Berlin Heidelberg, 2012) Chap. 25, p. 738.
[37] See Supplemental Material at http://link.aps.org/supplemental/10.1103/PhysRevB.102.195205 for a table of the TR-PL data fit parameters, as a function of β, and for an animated version of a larger subset (144 spectra) of the experimental data and corresponding $\beta = 1$ curve fits, from 0.5 to 200 ns.
[38] D. Mourad, J.-P. Richters, L. Gérard, R. André, J. Bleuse, and H. Mariette, Phys. Rev. B **86**, 195308 (2012).
[39] C. J. Hages, A. Redinger, S. Levcenko, H. Hempel, M. J. Koeper, R. Agrawal, D. Greiner, C. A. Kaufmann, and T. Unold, Adv. Energy Mater. **7**, 1700167 (2017).
[40] P. Virtanen *et al.*, Nat. Methods **1**7, 261 (2020).
[41] W. Gong, T. Tabata, K. Takei, M. Morihama, T. Maeda, and T. Wada, Phys. Status Solidi C: Current Topics in Solid State Phys. **12**, 700 (2015), 19th International Conference on Ternary and Multinary Compounds (ICTMC), Niigata, Japan, Sep 01–05, 2014.
[42] T. Gershon, K. Sardashti, O. Gunawan, R. Mankad, S. Singh, Y. S. Lee, J. A. Ott, A. Kummel, and R. Haight, Adv. Energy Mater. **6**, 1601182 (2016).
[43] Y. Jiang, B. Yao, J. Jia, Z. Ding, R. Deng, D. Liu, Y. Sui, H. Wang, and Y. Li, J. Appl. Phys. **125**, 025703 (2019).